Journal of Sound and Vibration (2001) **242**(5), 767–791
doi:10.1006/jsvi.2000.3379, available online at http://www.idealibrary.com on IDEAL®

ACTIVE POSITION CONTROL OF A FLEXIBLE SMART BEAM USING INTERNAL MODEL CONTROL

Y.-S. Lee and S. J. Elliott

Institute of Sound and Vibration Research, University of Southampton, Southampton SO17 1BJ, England.
E-mail: ysl@isvr.soton.ac.uk

(*Received* 8 *January* 1999, *and in final form* 15 *August* 2000)

The problem of controlling the position at the tip of a flexible cantilever beam to follow a command signal is considered, by using a pair of piezoelectric actuators at the clamped end. The beam is lightly damped and so the natural transient response is rather long, and also since the sensor and actuator are not collocated, the plant response is non-minimum phase. Two control strategies were investigated. The first involved conventional PID control in which the feedback gains were adjusted to give the fastest closed-loop response to a step input. The second control strategy was based on an internal model control (IMC) architecture. The control filter in the IMC controller was a digital FIR device designed to minimize the expectation of the mean square tracking error. In practice, such smart beams could be exposed to temperature fluctuations and changes in geometry. The effect of these variations on the stability was studied and it is shown that the need for robustness to such variations leads to a limitation in the performance of an IMC controller. The improvement in the stability robustness by incorporating control effort weighting into the cost function being minimized was investigated, as was the incorporation of modelling delay in the design of the IMC control filter. The IMC controller designed for the beam was found to have much reduced settling times to a step input compared with those of the PID controller while maintaining good robustness to changes in temperature. However, the extremely low damping of the experimental beam made it difficult to implement an accurate plant model in practice.

1. INTRODUCTION

Recent developments in smart materials such as piezoelectric zirconate titanate (PZT) ceramics and piezoelectric vinylidene fluoride (PVDF) polymer films enable actuators and sensors to be integrated into smart structures, which can then be controlled actively [1, 2]. The applications of such piezoelectric transducers have been investigated for smart structures for vibration rejection, using active vibration control (AVC), and sound radiation control of vibrating structures, using active structural acoustical control (ASAC), etc. [1, 2]. A new approach to tip position control of a flexible cantilever beam using PZT actuators is studied in this paper. This approach can be clearly distinguished from conventional vibration rejection controls in that the actuator is driven so that the beam tip follows a command signal. In practice, smart beams may be exposed to temperature fluctuations and variations in their payload. These effects will change the response of the beam and so could affect the stability and performance of a smart beam. Thus, the need to ensure robust stability in the face of the uncertainty in temperature and load leads to some limitations in the performance of a smart beam. Lightly damped flexible structures, such as the beam considered here, can have a long transient response when moved suddenly. However, some

0022-460X/01/200767 + 25 $35.00/0

mechanical systems consisting of flexible structures require high-speed and accurate tracking capabilities, such as robot manipulators in spacecrafts. In order to overcome the inherent long transient response of such structures, a feedforward control strategy could be used. The feedforward controller should anticipate the inverse dynamics of the plant within a specified bandwidth. The problem is made more difficult by the non-minimum phase behaviour of the system response, caused by the non-collocation of sensor and actuator, and the dispersive property of flexible structures. The non-minimum-phase zeros of the system response mean that an exact stable inverse cannot be achieved by direct inversion. A number of feedforward techniques have been developed to minimize the effect of unstable zeros on tracking performance of flexible manipulators [3–5]. An alternative formulation is presented here, in which a digital FIR filter is designed to minimize the mean-square tracking error. It is, however, well known that the performance of any feedforward strategy is sensitive to changes in the response of the system under control.

An alternative control strategy would be to use feedback control. Conventional analogue techniques, such as PID control, could be used, but the non-minimum phase behaviour limits the maximum control gains before there is a danger of instability, resulting in a rather long closed-loop transient response. A different feedback controller architecture is investigated here for the control of the flexible cantilever beam, which is known as internal model control (IMC), as described for example by Morari and Zafiriou [6]. The IMC architecture uses an internal model of the response of the system under control, the plant, and a control filter that can be designed to meet the control objectives of good tracking performance and robust stability. The IMC controller reduces to a feedforward system if the plant dynamics are known perfectly [6] and thus provides a connection with the earlier feedforward approach under nominal plant conditions. The robust stability of such a feedback controller to changes in the plant response can be assessed using a generalization of the complementary sensitivity function, which has a particularly simple form when IMC is used. The stability robustness can be improved by incorporating some effort weighting into the cost function being minimized [7]. It is shown that although the feedback nature of the IMC controller can cause instability if the changes in the plant response are too large, the performance of the closed-loop system is very much better than that of an entirely open-loop, feedforward, system before this limit is reached. Another method of making the feedforward controller into a closed-loop system would be to make it adaptive, and one method of achieving this is also discussed.

In most of the previous position control systems for flexible beams electrical motors have been the only actuator used, as for example, in references [3, 5]. In this paper, however, a pair of integrated piezoceramic (PZT) actuators is used, which provide many attractive features such as light weight, high sensitivity, large bandwidth and distributed properties [8, 9], although only limited motion is possible. For the sensing of the beam's motion, a non-contacting inductive position sensor was used. This sensor was chosen instead of an accelerometer since it does not affect the beam's motion and it directly measures displacement. A practical implementation of the IMC controller has also been investigated, which uses a floating-point 32-bit digital signal processor (DSP, TMS320C30), and the measured closed-loop performance has been compared with the predicted by a theoretical model.

2. EXPERIMENTAL ARRANGEMENT AND THEORETICAL BEAM MODEL

2.1. EXPERIMENTAL ARRANGEMENT

The experimental flexible beam was 800 mm long (L), 20 mm wide (B) and 1·5 mm thick (t), and was constructed of aluminium strip, clamped at one end and free at the other as

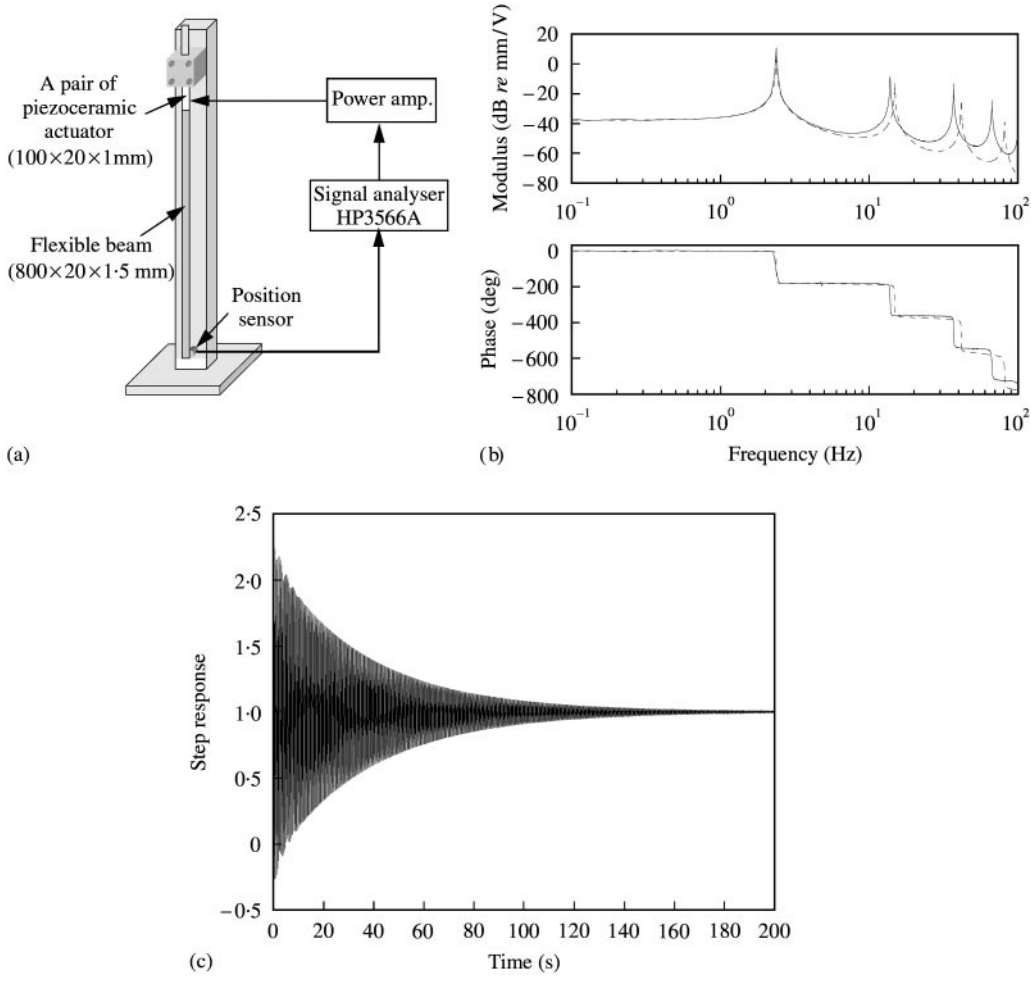

Figure 1. (a) The flexible cantilever beam used in the experiments and (b) its frequency response (tip deflection/input voltage), in which the solid line is the experimental result and the dashed line is a simulation result. (c) The measured step response of the experimental beam.

shown in Figure 1(a). A pair of "Morgan Matroc" PZT 5H type [10] piezoceramic actuators, which are each 100 mm long (L_a), 20 mm wide (B_a), and 1 mm thick (t_a), was bonded on either side of the beam at the clamped end and driven out of phase so as to generate a bending moment excitation. For the detection of the beam tip motion, an inductive position sensor (Honeywell proximity sensor 924 series 30 mm) which gives a linear sensitivity for the position control range of the beam was used. The frequency range of interest was 0–100 Hz and the beam positioned vertically for the experiment. The input voltage and the tip deflection were measured with an HP3566A Signal Analyzer, and the input signal to the piezoceramic actuator was amplified to 100 V by a PCB AVC 790 series power amplifier.

An initial system identification experiment was performed on the beam and Figure 1(b) shows the measured frequency response, where the input is the voltage to the piezoactuator and the output is the beam tip displacement. Four resonances were observed in the frequency range of interest, at 2·37 Hz, 13·92 Hz, 37·25 Hz, and 67·44 Hz respectively. Their

damping ratios were measured to be $\zeta_1 = 0{\cdot}0026$, $\zeta_2 = 0{\cdot}0036$, $\zeta_3 = 0{\cdot}00335$, and $\zeta_4 = 0{\cdot}0051$. The phase response shows a steep phase changes of -180° at each resonance frequency and, the phase delay of this beam system can be defined [11] to be

$$\tau_p(\omega) = -\varphi(\omega)/\omega, \tag{1}$$

where ω is the frequency and $\varphi(\omega)$ is the phase change. Both $\tau_p(\omega)$ and $\varphi(\omega)$ are also frequency dependent because the system is resonant. The average phase delay up to 100 Hz is about 30 ms. Figure 1(b) also indicates that the plant is dispersive and non-minimum phase, which is caused by the non-collocation of the actuator and sensor.

The measured steady state beam deflection was about 1·25 mm for 100 V step input to the piezoceramic actuators. The beam's response to a step input is shown in Figure 1(c), from which the 95 and 99% settling times were measured to be about 125 and 196 s respectively, emphasizing the very lightly damped nature of the beam.

2.2. DYNAMICS OF THE BEAM AND ACTUATOR

A uniform cantilever beam with length L which has clamped–free ends boundary conditions is considered and it is subjected to a harmonic bending moment $M(x, t)$ at $x = L_a$. The tip deflection $y(L, t)$ of the beam is assumed by the superposition of the individual flexural mode as

$$y(L, t) = \sum_{n=1}^{\infty} B_n(t)\phi_n(L), \tag{2}$$

where $B_n(t)$ is the nth flexural modal amplitude and $\phi_n(L)$ is the nth flexural mode shape at the tip which is given in reference [12]. By considering the boundary conditions of the cantilever beam, a receptance form for the tip deflection due to the bending moment at $x = L_a$ can be derived as

$$\frac{y(L)}{M(L_a)} = \sum_{n=1}^{\infty} \frac{k_n\phi_n(L)\phi_n'(L_a)}{A\rho L[(\omega_n^2 - \omega^2) + j2\zeta_n\omega_n\omega]}, \tag{3}$$

where k_n, ω_n, ζ_n are the nth flexural wavenumber, natural circular frequency, damping ratio of the beam, respectively, and $\phi_n'(L_a)$ is the spatial derivative of $\phi_n(x)$ at $x = L_a$, and A and ρ are the sectional area and the density of the beam respectively. A pair of piezoceramic elements bonded on either sides of the beam can induce bending moments at both ends ($x = 0$ and L_a) of the elements when they are driven out of phase. However, only the bending moment at $x = L_a$ will be applied to the beam because the beam is clamped at $x = 0$. The relationship between the bending moment M induced by a pair of piezoactuators and input voltage V is given as [10]

$$M = \alpha V, \tag{4}$$

where the coefficient α is the gain of the piezoceramic actuator. Thus, the relationship between the input voltage V and the tip deflection $y(L)$ or the transfer function of the "plant" model can be written in the Laplace domain as

$$G(s) = \frac{y(L)}{V} = K\sum_{n=1}^{\infty} \frac{a_n}{s^2 + 2\zeta_n\omega_n s + \omega_n^2}, \tag{5}$$

where $a_n = \phi_n(L)\phi'_n(L_a)$ and $K = \alpha k_n / A\rho L$ is the gain of the plant. The zeros of the plant model $G(s)$ depend on the coefficients a_n, which are determined by the phase relationship between the command input and the position output of the each resonant mode. In other words, the zeros, which have a direct effect on the overall stability of the control system [13], are dependent on the values of the mode shapes and the spatial derivatives of the mode shapes at L (location of sensor) and L_a (location of actuator). However, the poles are independent of the locations of the sensor and actuator since they correspond to the natural frequencies of the flexible beam system. The dashed line in Figure 1(b) is the frequency response of the flexible beam system predicted by using equation (5). Later in the paper, the effect of a small mass at the tip of the beam is discussed. The modal summation above was again used to model this system, but with the modified natural frequencies and mode shapes, as described by Laura *et al.* [14].

3. CONTROLLERS

3.1. ANALOGUE FEEDBACK CONTROLLERS

The block diagram of an analogue position control feedback system is shown in Figure 2(a), in which $r(t)$ is the command signal, $G(s)$ is the plant, $y(t)$ is the output of the plant, $e(t)$ is the error signal, and $u(t)$ is the control signal. One popular form of analogue controller is proportional, integral and derivative (PID) control for which

$$H(s) = K_P + \frac{K_I}{s} + K_D s, \tag{6}$$

where K_P is the proportional gain, K_I is the integral gain and K_D is the derivative gain.

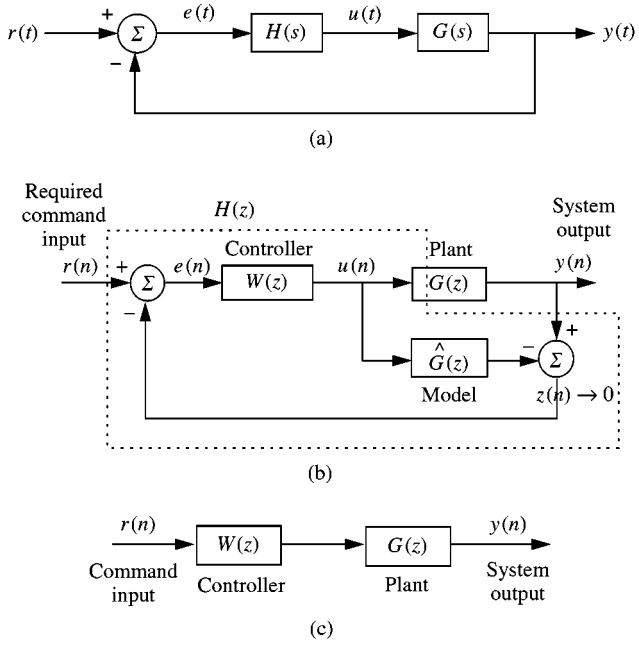

Figure 2. (a) Block diagram of an analogue position control feedback system. (b) Block diagram of IMC digital feedback control system for setpoint tracking. (c) An equivalent feedforward system to the IMC feedback control system when $\hat{G}(z) = G(z)$.

For a mechanical system such as the beam, the proportional term K_P will provide a bending moment input proportional to the tip displacement, and can thus be regarded as a form of electronic stiffness. The integral term ensures that the steady state tracking error is zero [15], and the derivative term provides a bending moment proportional to the velocity of the beam tip and can thus be thought of as providing active damping.

3.2. IMC FEEDBACK CONTROL

The internal model control (IMC) approach is a method of designing feedback control systems by using the mathematical techniques developed for feedforward control. IMC can transform a feedback position control system into a system resembling a feedforward position control system. Consider the block diagram of a digital IMC controller for a sampled-time single input, single output control system as shown in Figure 2(b). The digital feedback controller $H(z)$ contains an internal model $\hat{G}(z)$ of the real physical plant $G(z)$ and the control filter $W(z)$. The frequency response of the entire feedback controller is, thus

$$\frac{u(z)}{r(z) - y(z)} = H(z) = \frac{W(z)}{1 - W(z)\,\hat{G}(z)}. \tag{7}$$

The response of the output $y(n)$ of the entire feedback control system to the command signal $r(n)$ can also be expressed as

$$\frac{y(z)}{r(z)} = \frac{G(z)H(z)}{1 + G(z)H(z)} = \frac{W(z)G(z)}{1 + W(z)[G(z) - \hat{G}(z)]}. \tag{8}$$

If the plant model $\hat{G}(z)$ is a perfect representation of the plant $G(z)$ (i.e., $G(z) = \hat{G}(z)$) and $G(z)$ is stable, then the classical feedback system with controller $H(z)$ is internally stable if and only if $W(z)$ is stable [6] in which case $z(n)$ tends to zero in Figure 2(b) and the equivalent block diagram becomes entirely feedforward as shown in Figure 2(c). The system output $y(n)$ is then $W(z)G(z)r(n)$, and thus the complementary sensitivity function is equal to $W(z)G(z)$ in this case. Thus, if $W(z)$ is the inverse of $G(z)$, then the output $y(n)$ will follow the command signal $r(n)$ perfectly. In practice this cannot be achieved with a stable $W(z)$ since $G(z)$ is non-minimum phase and so a least-squares approximation to the inverse control could be used.

The more general problem of calculating the optimum performance of the feedforward system as shown in Figure 3(a) is outlined below, when the command signal $r(n)$ is fed to an FIR feedforward digital filter $W(z)$, with I coefficients, whose output drives the digital plant $G(z)$ and the plant then produce the system output $y(n)$. The desired signal $d(n)$ is equal to the command signal $r(n)$ delayed by Δ samples. Such a *modelling delay* is not generally used in control systems since the required signal may not be known in advance in all applications, and to aid comparison with other feedback controllers in section 3, Δ will initially be taken to be zero. In some applications, however, such as when the plant is required to execute a repetitive motion for example, the required signal is known in advance, and considerable improvements in performance can be obtained with a suitable choice of Δ, which is known as the modelling delay in the signal processing literatures [16].

The error signal $e(n)$ can be given by subtracting the system output $y(n)$ from the desired signal $d(n)$ as

$$e(z) = d(z) - W(z)G(z)r(z). \tag{9}$$

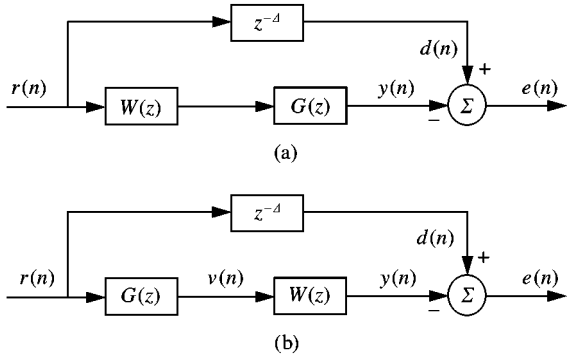

Figure 3. (a) Block diagram of a feedforward control system to track a setpoint command. (b) Rearrangement of block diagram for the design of the optimal control filter $W(z)$.

However, if the control filter $W(z)$ is fixed and is linear time invariant, the order of the blocks $G(z)$ and $W(z)$ can be reversed, as shown in Figure 3(b), to generate a signal $v(n)$ which is equal to the command signal filtered by the digital plant $G(z)$. Since the control filter is a FIR filter device the error signal can now be expressed [17] as

$$e(n) = d(n) - \mathbf{w}^{\mathrm{T}}\mathbf{v}(n), \tag{10}$$

where $\mathbf{w} = [w_0 \cdots w_{I-1}]^{\mathrm{T}}$, w_i is the ith coefficient of the control filter $W(z)$ and $\mathbf{v}(n) = [v(n) \cdots v(n - I + 1)]^{\mathrm{T}}$. Upon assuming that the reference signal is random each w_i can be adjusted to minimize a cost function J_1 equal to the expectation of square values of the error signals $e(n)$ and so

$$J_1 = E[e^2(n)]. \tag{11}$$

The expectation of the squared error signals can now be written as

$$E[e^2(n)] = \mathbf{w}^{\mathrm{T}}\mathbf{A}\mathbf{w} - 2\mathbf{w}^{\mathrm{T}}\mathbf{b} + c, \tag{12}$$

where c is the scalar $E[d^2(n)]$, $\mathbf{b}$ is the vector of cross-correlation function between $\mathbf{v}(n)$ and $\mathbf{d}(n)$, $\mathbf{b} = E[\mathbf{v}(n)\,d(n)]$ and $\mathbf{A}$ is a Toeplitz matrix of auto-correlation function of v as $\mathbf{A} = E[\mathbf{v}(n)\mathbf{v}^{\mathrm{T}}(n)]$. If $\mathbf{A}$ is not singular, the matrix equation can be solved for the optimal, Wiener, set of filter coefficients $\mathbf{w}_{opt}$ which will produce a minimum error signal as

$$\mathbf{w}_{opt} = \mathbf{A}^{-1}\mathbf{b}. \tag{13}$$

This Wiener filter can then be readily calculated from the cross-correlation vector and the auto-correlation matrix.

The numerical stability of the solution of equation (13) depends on the conditioning of the matrix $\mathbf{A}$, because this optimal Wiener solution depends on its inverse. The conditioning may be improved by modifying the cost function to add a regularization term that is proportional to the expectation of the squared values of the filter coefficients [7], so that

$$J_2 = E[e^2(n)] + \beta\mathbf{w}^{\mathrm{T}}\mathbf{w}, \tag{14}$$

in which case the Hessian matrix becomes $\mathbf{A} = E[\mathbf{v}(n)\mathbf{v}^{\mathrm{T}}(n) + \beta\mathbf{I}]$, when written in Hermitian quadratic form, in which the coefficient weighting or regularization parameter

β improves the condition number of the **A** matrix to be inverted and **I** means an identity matrix. Thus, the optimal set of coefficients in equation (13) can be re-expressed as

$$\mathbf{w}_{\beta,opt} = \{E[\mathbf{v}(n)\mathbf{v}^{\mathrm{T}}(n) + \beta\mathbf{I}]\}^{-1}E[\mathbf{v}(n)\,d(n)]. \tag{15}$$

3.3. ROBUST STABILITY

The IMC architecture has an evident danger: that its stability may be extremely sensitive to the accuracy of the plant model. H_∞ control techniques [18] enable the robust stability of the IMC position controller to be assessed analytically. For the design of a robustly stable system which will not be unstable when the plant response changes within given bounds, the uncertainty of the plant must be considered. If the uncertainty is expressed with a multiplicative factor, the frequency response of the digital plant can be written as

$$G(\mathrm{e}^{\mathrm{j}\omega\mathrm{T}}) = [1 + \Delta_G(\mathrm{e}^{\mathrm{j}\omega\mathrm{T}})]\,G_0(\mathrm{e}^{\mathrm{j}\omega\mathrm{T}}), \tag{16}$$

where $G_0(\mathrm{e}^{\mathrm{j}\omega\mathrm{T}})$ is the frequency response of the nominal plant, $\Delta_G(\mathrm{e}^{\mathrm{j}\omega\mathrm{T}})$ is the fractional change in the plant frequency response, and T is the sample time. The bound of the magnitude of the multiplicative plant uncertainty is

$$|\Delta_G(\mathrm{e}^{\mathrm{j}\omega\mathrm{T}})| < B(\mathrm{e}^{\mathrm{j}\omega\mathrm{T}}), \tag{17}$$

where $|\Delta_G(\mathrm{e}^{\mathrm{j}\omega\mathrm{T}})|$ denotes the modulus of $\Delta_G(\mathrm{e}^{\mathrm{j}\omega\mathrm{T}})$ and the real but potentially frequency-dependent quantity $B(\mathrm{e}^{\mathrm{j}\omega\mathrm{T}})$ is the upper bound of the uncertainty. If the complementary sensitivity function $T_0(\mathrm{e}^{\mathrm{j}\omega\mathrm{T}})$ is defined as

$$T_0(\mathrm{e}^{\mathrm{j}\omega\mathrm{T}}) = \frac{G_0(\mathrm{e}^{\mathrm{j}\omega\mathrm{T}})H(\mathrm{e}^{\mathrm{j}\omega\mathrm{T}})}{1 + G_0(\mathrm{e}^{\mathrm{j}\omega\mathrm{T}})H(\mathrm{e}^{\mathrm{j}\omega\mathrm{T}})}, \tag{18}$$

then the condition for robust stability is guaranteed if

$$\| T_0(\mathrm{e}^{\mathrm{j}\omega\mathrm{T}})B(\mathrm{e}^{\mathrm{j}\omega\mathrm{T}})\|_\infty < 1, \tag{19}$$

where $\| T_0(\mathrm{e}^{\mathrm{j}\omega\mathrm{T}})B(\mathrm{e}^{\mathrm{j}\omega\mathrm{T}})\|_\infty$ is the largest value of $|T_0(\mathrm{e}^{\mathrm{j}\omega\mathrm{T}})B(\mathrm{e}^{\mathrm{j}\omega\mathrm{T}})|$ at any frequency. Provided equation (19) is satisfied, the control system will stay stable for any plant response which satisfies equations (16) and (17). If IMC control is used with a plant model equal to the nominal plant response, so that $\hat{G}(\mathrm{e}^{\mathrm{j}\omega\mathrm{T}}) = G_0(\mathrm{e}^{\mathrm{j}\omega\mathrm{T}})$, then the condition for robust stability can be expressed by using equations (7) and (18) as [6]

$$|W(\mathrm{e}^{\mathrm{j}\omega\mathrm{T}})G_0(\mathrm{e}^{\mathrm{j}\omega\mathrm{T}})B(\mathrm{e}^{\mathrm{j}\omega\mathrm{T}})| < 1 \quad \text{for all } \omega. \tag{20}$$

If an effort weighting β is introduced into the cost function in equation (15), the magnitude of the frequency response of the control filter, $|W(\mathrm{e}^{\mathrm{j}\omega\mathrm{T}})|$, will also tend to be reduced, thus satisfying the condition for robust stability, equation (19) for higher values of plant uncertainty, $B(\mathrm{e}^{\mathrm{j}\omega\mathrm{T}})$ and making the controller more robust.

4. CONTROL SIMULATION

4.1. INTRODUCTION

For the control simulation, the length of the analytic beam model was assumed to be $L = 723$ mm for the prediction in order to match with the measured first natural frequency

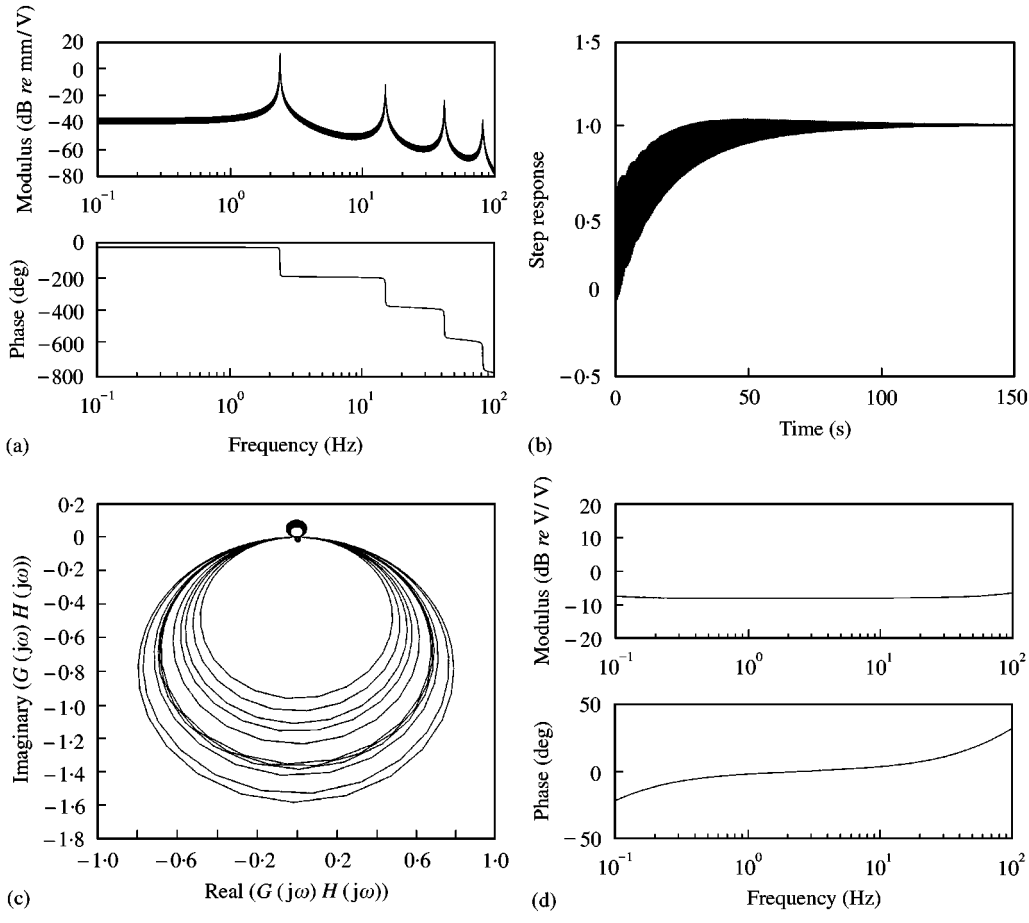

Figure 4. Simulation of PID feedback control with plant uncertainty. (a) The effect of structured uncertainty due to temperature changes on the frequency response of the flexible beam. (b) Step response of the closed-loop system with the nominal plant (at $T = 20°C$). (c) Nyquist plot with plant uncertainty where the outermost line is 70°C and the innermost line is $-30°C$. (d) Frequency response of the PID controller.

shown as the dashed lines in Figure 1(b). This can be justified because of the stiffening effect of the piezoceramic actuators. The modal damping ratio ζ_n used in simulation for the prediction was taken from the experimental measurements.

In practice, smart structures with piezoelectric transducers may be exposed to significant temperature fluctuations. An analysis has thus been performed on the effect of the temperature fluctuations on the response of the beam. In this study, in order to assess the effect of such changes, or uncertainty, in the plant on the stability and performance of the controller, temperature variations between -30 and 70°C have been assumed in the plant model, while the nominal temperature was 20°C. Temperature changes will cause changes in the value of piezoelectric constant d_{31} of the PZT 5H and of the beam length. The value of d_{31} is about $2{\cdot}74 \times 10^{-10}$ N/m^2 at the nominal temperature (20°C); however, it varies to about $3{\cdot}20 \times 10^{-10}$ N/m^2 at 70°C and about $1{\cdot}95 \times 10^{-10}$ N/m^2 at $-30°C$ [10]. This change of d_{31} is proportional to change in the magnitude of the induced bending moment M [9], which affects the gain of the plant frequency response, and the change of the beam length affects the resonance frequencies of the plant. Figure 4(a) shows the effect of these

temperature changes on the modelled plant response, and it can be seen that the change in beam length gives only a small effect compared with that of the gain, since very little phase change is observed in the plant frequency response. Figure 4(a) also shows that when the temperature rises, the gain of the plant becomes larger and when the temperature falls, the gain becomes smaller. In addition to these temperature variations, a small variable tip mass has also been introduced (0–0·5% of the beam mass) to further investigate the stability of the control system when the natural frequency of the plant is uncertain. The maximum tip mass investigated (0·5% of the beam mass) resulted in a decrease in the first natural frequency of about 0·023 Hz which is about 1% of the unperturbed first natural frequency.

In this section, simulation with three different control strategies with a PID feedback controller (see section 4.2), an IMC feedback controller using various conditions (see sections 4.3–4.6), and an adaptive feedforward controller using filtered-x LMS algorithm (see section 4.7) will be discussed in detail. The summarized control simulation results, presented in advance in Table 1, show the comparison of performance and stability on each controller, where GM is a gain margin, PM is a phase margin and t_s indicates a settling time.

4.2. PID CONTROL SIMULATION

In the PID feedback control simulation, an analogue controller with three gain terms ($K_P = 0{\cdot}4$, $K_I = 1{\cdot}6$, and $K_D = 0{\cdot}0004$) which were manually tuned to give the fastest step response and adequate stability margins in experiment was considered. The PID control in simulation showed a very high gain margin due to the lightly damping and a phase margin of about 44°, as shown in Figure 4(c). The stability was dominantly dependent on the open-loop behaviour of the first resonance. 95 and 99% settling times in step response were about 67 and 146 s, respectively, as shown in Figure 4(b). Figure 4(c) indicates the Nyquist plot of the open-loop frequency response of the PID control, for various temperatures in 10°C intervals from -30 to 70°C. A rise in temperature causes the phase margin to fall from about 44 (nominal, $T = 20$°C) to about 37° (perturbed, $T = 70$°C) as shown in Table 1. The closed-loop step response of the PID feedback control is not significantly affected by these temperature changes of the beam. A tip mass variation between 0 and 0·5% of the beam mass also had almost no effect on the stability and performance of the PID control as summarized in Table 2. Figure 4(d) shows the frequency response of the PID controller $H(s)$, in which the integral action is clear below 0·1 Hz and the derivative action is evident only near 100Hz.

4.3. IMC CONTROL SIMULATION WITH THE NOMINAL PLANT

For IMC control simulations, the plant was transformed into digital form with a sample rate of 300 Hz by using the matched pole-zero method [15]. The digital IMC feedback control was then simulated with the nominal plant, when $G(z) = \hat{G}(z) = G_0(z)$, which is equivalent to the purely feedforward control illustrated in Figure 2(c). The optimal control filter $W(z)$ was designed with a 200 coefficients FIR filter to minimize the mean square error between the plant output and "Brownian noise" as a command signal. Brownian noise was chosen because its power spectral density has the same form as the modulus squared spectrum of a step function and it was generated by cumulatively summing a white-noise signal, so that

$$r(n) = x_B(n) = \sum_{i=1}^{n} x_W(i), \tag{21}$$

TABLE 1

Summary of control simulation results of a PLD feedback controller, an IMC feedback controller (with various conditions) and an adaptive feedforward controller (filtered-x LMS)

Controller	Stability	Nominal plant	Perturbed plant	
			Response	Temperature (°C)
PID feedback	Stable at $-30-+70$°C	GM = very high PM = 44° 95% $t_s = 67$ s 99% $t_s = 146$ s	GM = very high PM = 37° 95% $t_s = 67$ s 99% $t_s = 146$ s	70
IMC feedback (No Δ, No β)	Stable at $-30-+47$°C	GM = 6·5 dB PM = 38·0° 95% $t_s = 0{\cdot}10$ s 99% $t_s = 0{\cdot}62$ s	GM = 6·2 dB PM = 11·0° 95% $t_s = 0{\cdot}62$ s 99% $t_s = 1{\cdot}72$ s	40
IMC feedback (No Δ, $\beta = 10^{-7}$)	Stable at $-30-+47$°C	GM = 6·5 dB PM = 38·0° 95% $t_s = 0{\cdot}11$ s 99% $t_s = 0{\cdot}62$ s	GM = 6·2 dB PM = 10·9° 95% $t_s = 1{\cdot}73$ s 99% $t_s = 2{\cdot}14$ s	40
IMC feedback ($\Delta = 100$, No β)	Stable at $-30-+70$°C	GM = 6·0 dB PM = 60·0° 95% $t_s = 0{\cdot}42$ s 99% $t_s = 0{\cdot}42$ s	GM = 4·1 dB PM = 53·4° 95% $t_s = 0{\cdot}66$ s 99% $t_s = 1{\cdot}14$ s	70
Adaptive feedforward (filtered-x LMS)	Stable at $-30-+70$°C	Stability guaranteed 95% $t_s = 0{\cdot}55$ s 99% $t_s = 21{\cdot}14$ s	Stability guaranteed 95% $t_s = 0{\cdot}55$ s 99% $t_s = 22{\cdot}01$ s	70

TABLE 2

Simulation results of the stability comparison of PID feedback and IMC feedback controls when the plant is varied with its tip mass (0–0·5% of beam mass); IMC control filters are designed with different modelling delays Δ; O and X represent "stable" abd "unstable" respectively

Control		Tip mass (per cent of beam mass)				
		0%	0·1%	0·2%	0·3%	0·5%
PID feedback		O	O	O	O	O
IMC feedback	$\Delta = 0$	O	O	X	X	X
	$\Delta = 20$	O	O	X	X	X
	$\Delta = 50$	O	O	O	X	X
	$\Delta = 100$	O	O	O	O	X

where $x_B(n)$ is a Brownian noise sequence and $x_W(n)$ is a zero-mean white-noise sequence. In general, a persistently exciting [19] input signal is used for the design of an optimal filter [17]. However, a tracking control filter requires a good "integration action" to make a system follow the command position and so Brownian noise, which is particularly "spectrally rich" at low frequencies, provides a suitable training signal.

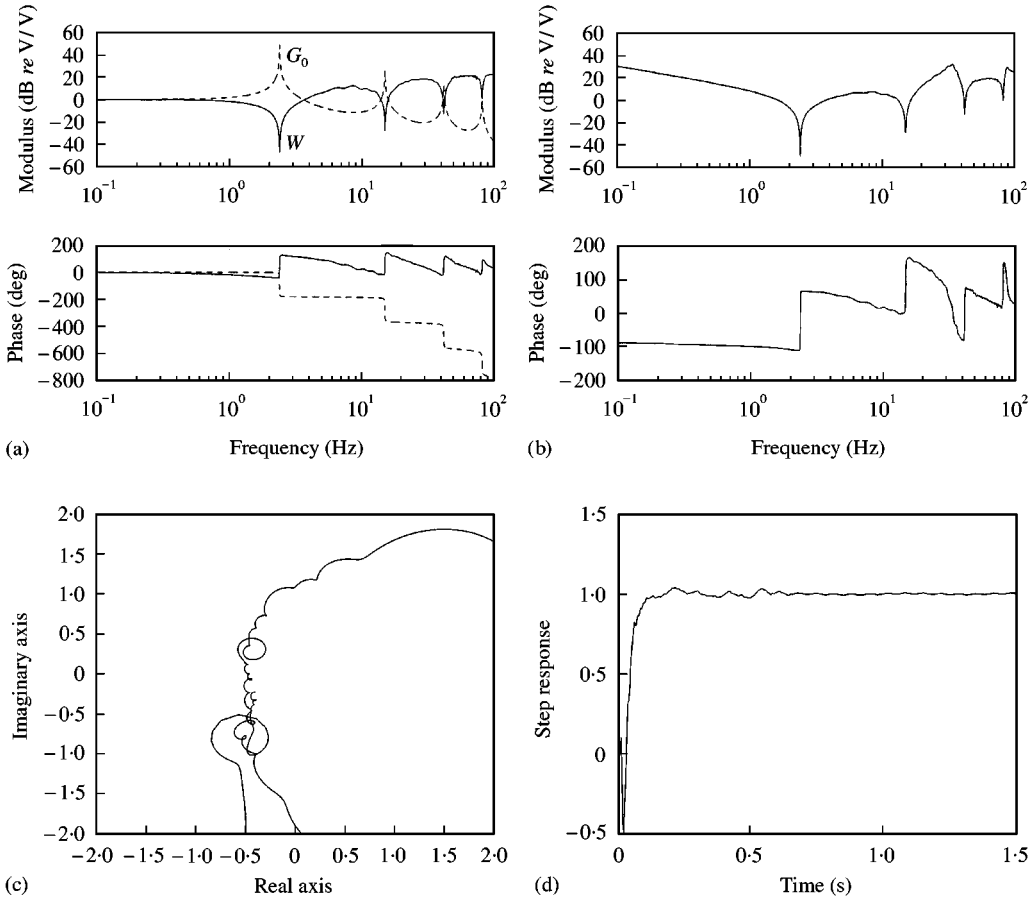

Figure 5. Simulation results for IMC feedback control with the nominal plant when $G(z) = \hat{G}(z) = G_0(z)$. (a) Frequency responses of $G_0(z)$ (– – – –) and $W(z)$ (—). (b) Frequency response of $H(z)$. (c) Nyquist plot, in which the "∗" is the Nyquist point at $(-1, 0)$. (d) Step response.

The frequency response of $W(z)$, the designed control filter, is shown in Figure 5(a) and represents the optimum stable form of the inverse dynamics of the plant, which has zeros cancelling each resonance of the plant. The frequency response of the entire feedback controller $H(z)$ shown in Figure 5(b), and has a high gain integral action at the low-frequency range, especially below the first resonance. The 95 and 99% settling times of the closed-loop step response were 0·10 and 0·62 s, respectively, as shown in Figure 5(d) and Table 1 (IMC feedback, No Δ, No β, for nominal plant). In spite of this fast settling, the IMC controller still has a gain margin of about 6·5 dB and a phase margin of about 38°, as can be seen from the Nyquist plot at Figure 5(c).

4.4. IMC CONTROL SIMULATION WITH PERTURBED PLANTS

The stability and performance of the IMC controller for perturbed plant conditions due to temperature variations were assessed by assuming that $\hat{G}(z) = G_0(z)$ and that the control filter $W(z)$ was designed for the nominal plant. The simulation results show that the IMC control is more sensitive than PID control. This is because the IMC control filter $W(z)$ is

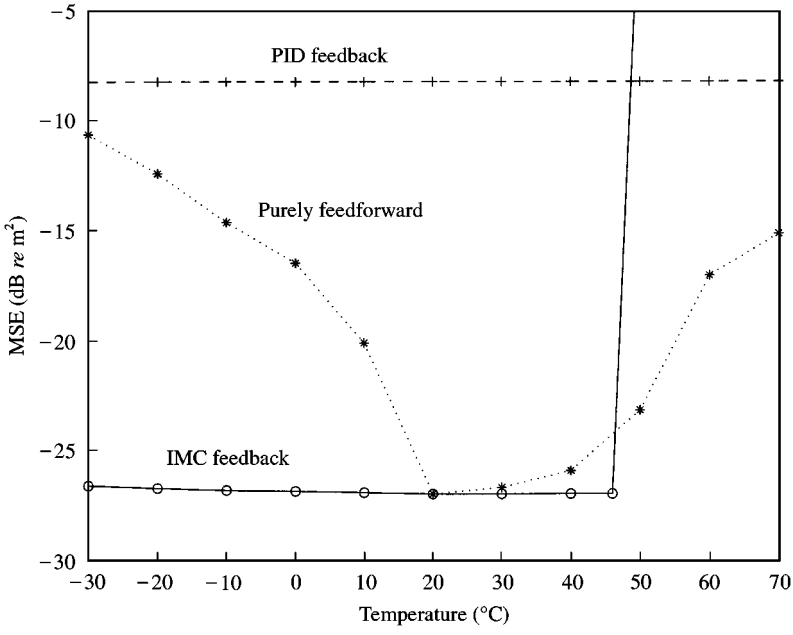

Figure 6. Variation of the mean-square tracking error (MSE) for a step input due to the temperature changes of the beam using three different controllers.

designed to invert the response of the nominal plant $G_0(z)$, whereas the PID controller has a relatively flat frequency response. Figure 6 shows the variation of the mean square tracking error (MSE) in the step response against temperature variation of the plant with three different controllers (PID, purely feedforward, and IMC). The performance of the PID controller is almost unaffected by the temperature changes, although MSE is only about -8 dB even for the nominal plant. The performance of the purely feedforward controller quickly degenerates as the temperature changes, because the inverse of the nominal plant is not well matched to perturbed plants. The feedback loop provided by the IMC controller reduces this degeneration significantly, and the MSE was changed by less than 1 dB for temperature of -30 to about 47°C. However, the disadvantage of closed-loop controller is that it can become unstable if the response of the plant changes too much, whereas the open-loop controller is unconditionally stable. The IMC controller becomes unstable if the beam temperature is above about 48°C, which is plotted in Figure 6 as having a very large tracking error.

The way in which the IMC controller becomes less stable as the temperature rises is shown in Figure 7. Figure 7(a) shows the feedforward responses of both $G_0(z)W(z)$ at $T = 20$°C (dashed line) and $G(z)W(z)$ at $T = 40$°C (solid line) when the control filter $W(z)$ was designed for the nominal plant. As shown in Figure 7(b), the Nyquist plot for the perturbed plant is much closer to the Nyquist point, although the gain margin is only reduced from 6·5 (nominal) to 6·2 dB (perturbed). The phase margin, however, has decreased from about 38 (nominal) to about 11° (perturbed) as summarized in Table 1 for this simulation (IMC feedback, No Δ, No β, for perturbed plant). The effect of this reduction of gain and phase margins is to make the complementary sensitivity functions much larger at the first resonance, as shown in Figure 7(c). The step response (99% settling time: 1·73 s), however, is not greatly affected by this increase of temperature, as shown in Figure 7(d) and Table 1. The stability robustness of the IMC controller with variations in beam tip mass is again indicated, for $\Delta = 0$, in Table 2.

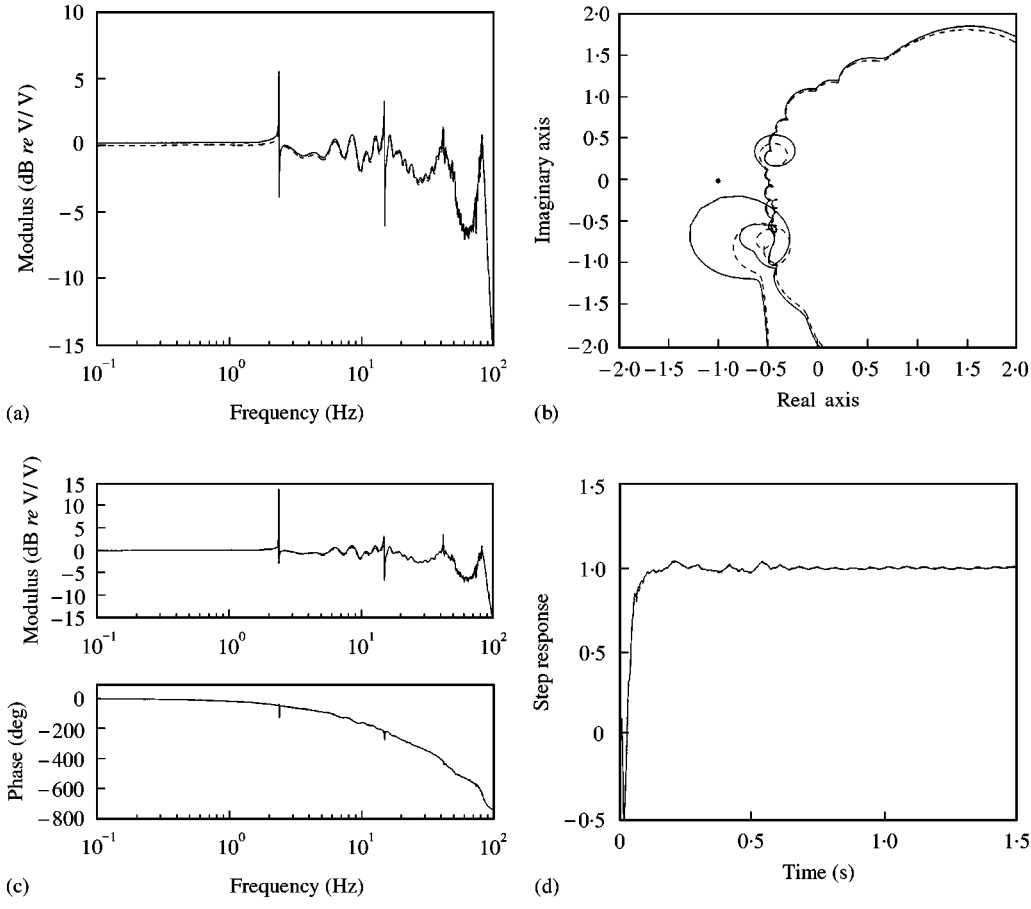

Figure 7. Comparison of the responses of the IMC feedback control for the nominal plant $G_0(z)$ ($T = 20°C$, – – – –) and perturbed plant $G(z)$ ($T = 40°C$, —). (a) $G_0(z)W(z)$ and $G(z)W(z)$. (b) $G_0(z)H(z)$ and $G(z)H(z)$. (c) $T_0(z)$ (nominal) and $T(z)$ (perturbed). (d) Step responses.

4.5. IMC CONTROL SIMULATION WITH CONTROL EFFORT FOR PERTURBED PLANTS

In order to increase the stability robustness, the IMC feedback controller could be redesigned by adjusting the control filter $W(z)$ to minimize the modified cost function J_2 in equation (14), with control effort weighting β, as successfully applied to active noise control systems [7, 20]. The value of β can be increased until the IMC feedback controller has the required degree of robust stability, but this will inevitably degrade the closed-loop performance. Thus, the trade-off between the performance and robust stability of the IMC feedback control is important in the design of the control filter $W(z)$.

Figure 8 illustrates the comparison of the IMC feedback control when control filters are either $W_\beta(z)$ with $\beta = 10^{-7}$ or $W(z)$ without β for a perturbed plant ($T = 40°C$). The frequency responses of $W_\beta(z)$ and $H_\beta(z)$ have a reduced modulus especially in the higher frequencies, the stability was increased slightly (GM = 6·5 dB, PM = 10·9°), but the step response becomes slightly slower (95 and 99% settling times: 1·73 and 2·14 s) as shown in Figure 8. Thus, the stability is only slightly more robust, in spite of the sacrifice of the

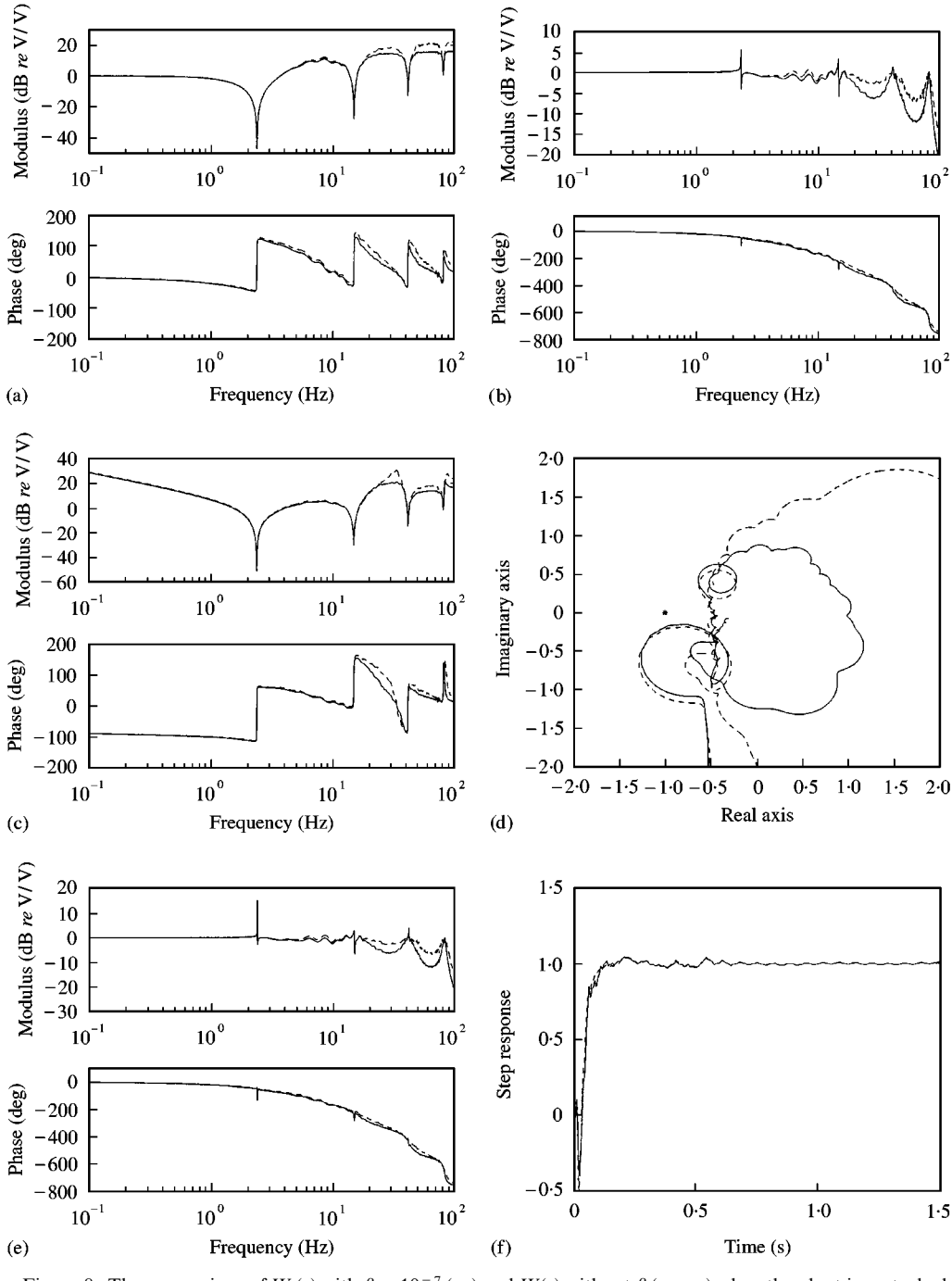

Figure 8. The comparison of $W_\beta(z)$ with $\beta = 10^{-7}$ (—) and $W(z)$ without β (– – – –) when the plant is perturbed ($T = 40°C$). (a) $W_\beta(z)$ and $W(z)$. (b) $G(z)W_\beta(z)$ and $G(z)W(z)$. (c) $H_\beta(z)$ and $H(z)$. (d) $G(z)H_\beta(z)$ and $G(z)H(z)$. (e) $T_\beta(z)$ and $T(z)$. (f) Step responses.

performance as summarized in Table 1 (IMC feedback, No Δ, $\beta = 10^{-7}$). For the nominal plant, the control filter $W_\beta(z)$ with $\beta = 10^{-7}$ gave 95 and 99% settling times of 0·11 and 0·62 s, respectively, without changes in gain margin and phase margin.

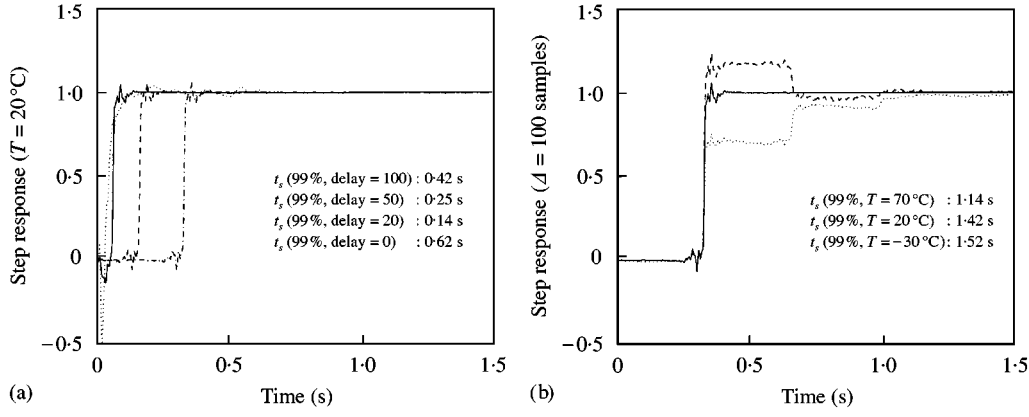

Figure 9. (a) The comparison of step responses by the IMC control filters with different modelling delays (Δ = 0, 20, 50, and 100) for the nominal plant (T = 20°C): , dealy = 0; —, delay = 20; – –, delay = 50; –, delay = 100. (b) A comparison of step responses for perturbed plants (T = − 30 and 70°C) and the nominal plant (T = 20°C) using the same control filter $W(z)$ designed with Δ = 100: , −30°C; —, 20°C; – –, 70°C.

Further increases in β were found to make the perturbed control system become unstable, and so the effort weighting parameter must be carefully chosen. Thus, the use of effort weighting does not appear to be a useful way of making this position feedback control of the flexible beam robust. This is because the stability of the IMC feedback control is mainly determined by the response of the first natural frequency as shown in Figure 8(d).

4.6. IMC CONTROL SIMULATION WITH MODELLING DELAYS FOR PERTURBED PLANTS

A modelling delay in the desired signal, as shown in Figure 3, allows the design of the control filter $W_\Delta(z)$ with a much smaller mean square tracking error (MSE). Figure 9(a) shows that the step responses of the nominal plant with control filters $W_\Delta(z)$ designed for modelling delays of Δ = 0, 20, 50, and 100 samples. Apart from the overall delay of the plant $G(z)$, the control filter designed with a modelling delay gave a faster settling than that designed without Δ. A comparison of the step responses of the control filter $W_\Delta(z)$ (Δ = 100) for perturbed plants (at T = − 30 and 70°C) and the nominal plant is illustrated in Figure 9(b). With a modelling delay of Δ = 100 the IMC feedback control becomes stable even for a perturbed plant at T = 70°C and is thus considerably made robust than the IMC control with Δ = 0. The step response with Δ = 100 for a temperature of T = 70°C shows an overshoot with a fast rise time at the initial stage, in contrast to a low temperature, T = − 30°C, which shows a fast rise time without an overshoot. The initial errors in step responses for both cases occurred due to the action of feedforward path, when the IMC feedback control was not effective. However, in both cases the error is gradually corrected by the feedback action in IMC feedback structure.

The MSE for perturbed plant responses is plotted against temperature variation in Figure 10 for various modelling delays. Figure 10 indicates that the IMC feedback control becomes more robust and could provide good tracking performance when the modelling delay is applied in the design of the control filter $W_\Delta(z)$.

Figure 11 compares the IMC control for the plant at T = 70°C when the control filter is either $W_\Delta(z)$ (Δ = 100, solid lines) or $W(z)$ (Δ = 0, dashed lines). The modulus of $G(z)W_\Delta(z)$ over the first natural frequency became less resonant, which appears as large circles in the

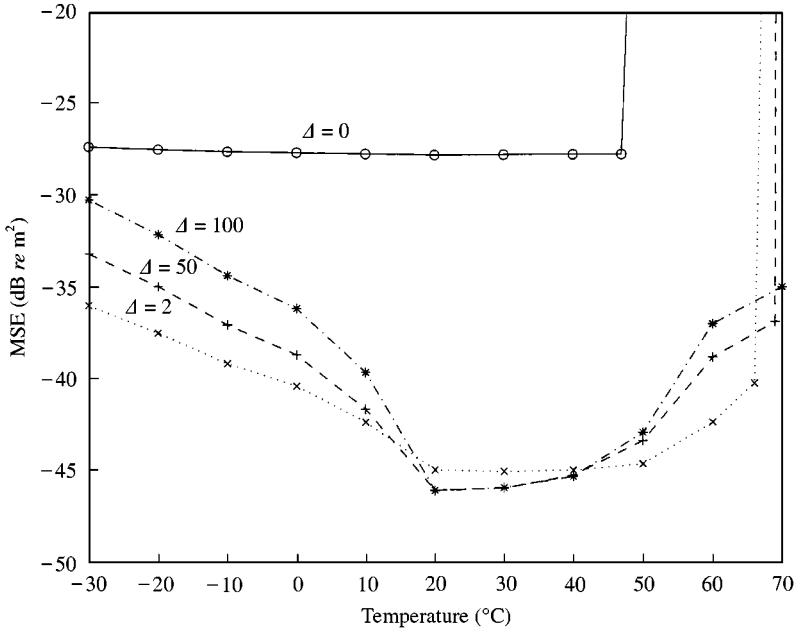

Figure 10. The mean-square tracking errors (MSE) of IMC feedback control against perturbed plants ($T = -30°C - +70°C$) with various modelling delays in the design of control filter $W(z)$.

Nyquist plot shown in Figure 11(d). The entire feedback controller, $H_{\Delta}(z)$, has a lower gain by about 20 dB compared with $H(z)$ in low frequencies. Thus, the unstable control system at $T = 70°C$ with $W(z)$ became stable with $W_{\Delta}(z)$. The results for this simulation (IMC feedback, $\Delta = 100$, No β) are summarized in Table 1.

The stability of the IMC controller using the control filter designed with a modelling delay has also been assessed for various tip masses. As can be seen from Table 2, an increase of modelling delay Δ gives better stability. However, since the IMC control is based on an internal nominal plant model, the IMC feedback control has less stability robustness than that of PID control.

4.7. ADAPTIVE FEEDFORWARD TRACKING CONTROL

Another way of compensating for a changing plant response is to use an adaptive feedforward control filter. Such an arrangement for the setpoint tracking problem is illustrated in Figure 12, in which the filter is adapted using the filtered-x LMS [16] algorithm. In Figure 12, $G(z)$ is the physical plant, which can vary with temperature, $\hat{G}(z)$ is the plant model at $T = 20°C$, $W(z)$ is the adaptive FIR control filter with 200 coefficients, $z^{-\Delta}$ is a modelling delay included for generality, although in this case is $\Delta = 0$, $r(n)$ is the command signal, $d(n)$ is the desired signal, $y(n)$ is the plant output signal $\hat{v}(n)$ is the filtered command signal and $e(n)$ is the error signal. The update equation of the filtered-x LMS algorithm is given by

$$\mathbf{w}_{n+1} = \mathbf{w}_n + \alpha \hat{\mathbf{v}}(n) e(n), \tag{22}$$

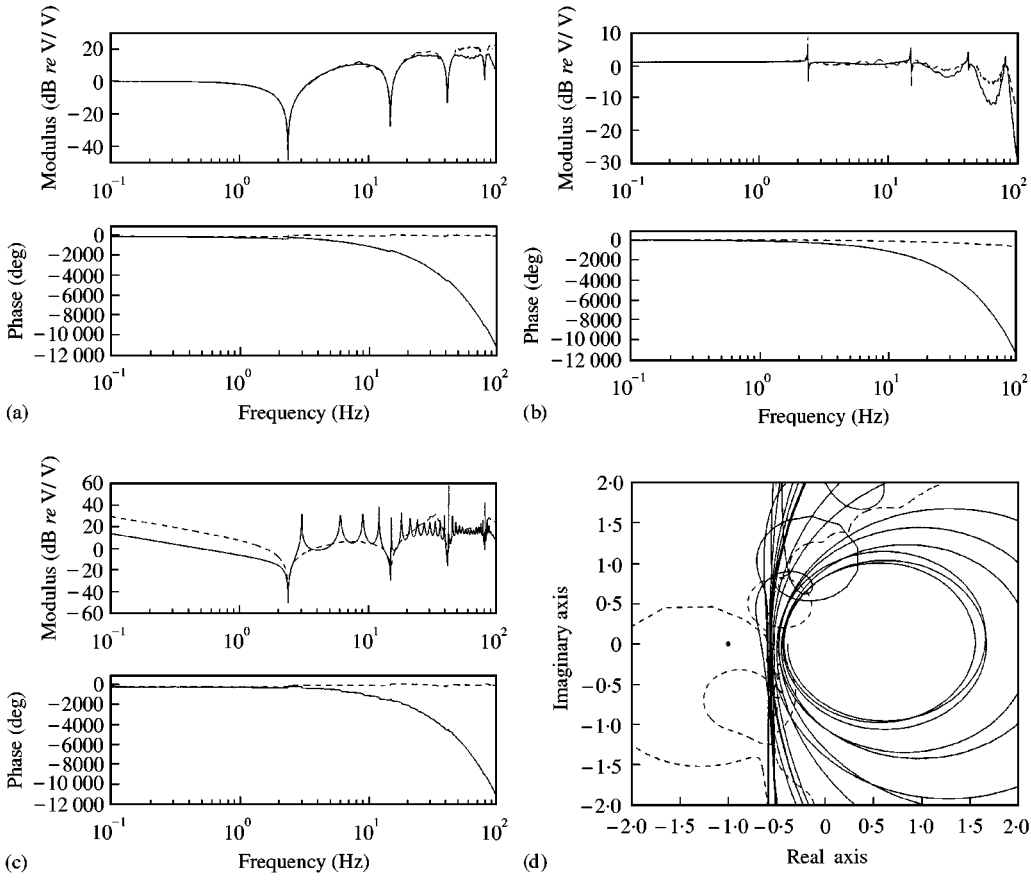

Figure 11. The comparison of the responses of the IMC feedback control for a "hot" plant at $T = 70°C$ when the control filters $W_\Delta(z)$ and $W(z)$ are designed both with (—) and without (– – – –) modelling delay of $\Delta = 100$ respectively. (a) $W_\Delta(z)$ and $W(z)$. (b) $G(z)W_\Delta(z)$ and $G(z)W(z)$. (c) $H_\Delta(z)$ and $H(z)$. (d) $G(z)H_\Delta(z)$ and $G(z)H(z)$.

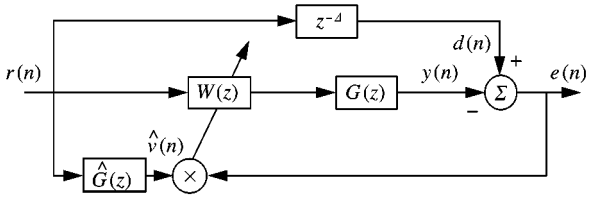

Figure 12. Arrangement of filtered-x LMS algorithm for the adaptive feedforward tracking control of the flexible beam with plant uncertainty.

where α is a convergence coefficient and $\mathbf{w}$ is the vector of LMS adaptive filter coefficients. For the tracking control of the flexible beam, the convergence coefficient α chosen to be in the range is expressed as

$$0 < \alpha < \alpha_0 / IE[\hat{v}^2(n)], \tag{23}$$

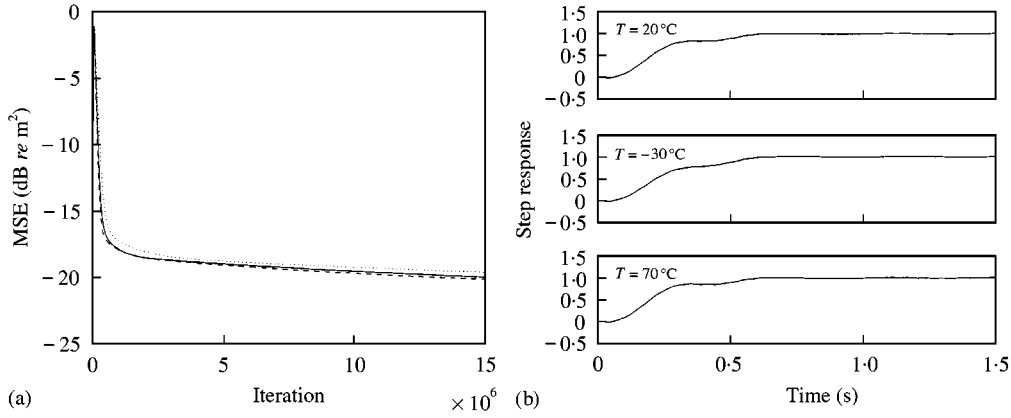

Figure 13. Simulation of adaptive feedforward control using the filtered-x LMS algorithm for a flexible beam. (a) Learning curves with three different temperatures of $T = 20°C$ (—), $-30°C$ (·····), and 70°C (– – – –). (b) Step responses after adaptation at three different temperatures at $T = 20°C$ (top), $-30°C$ (middle) and 70°C (bottom).

where I is the number of adaptive filter coefficients and α_0, representing the normalized convergence coefficient, is typically 10^{-6}, because of the very large phase delays in the plant at the first resonance.

The learning curves for the system with three different temperatures of $T = 20$, -30 and 70°C are shown in Figure 13(a) and were not entirely finished by 15×10^6 iterations for the adaptation, because of the low value of α which caused slow convergence, and the MSE had reached only about -20 dB. However, the learning curves of the three different plants showed similar convergence behaviour. Figure 13(b) illustrates the step responses after adaptation for 15×10^6 iterations for the three different plants. The settling times of the three step responses are similar as summarized in Table 1 (adaptive feedforward). The filtered-x LMS adaptive filter could provide a better performance than that presented with even more iterations but at a sampling rate of 300 Hz, 15×10^6 iterations would take about 14 h in real time.

5. EXPERIMENTAL RESULTS

5.1. ANALOGUE PID FEEDBACK CONTROL

Two position-control experiments for the flexible beam were performed, with either an analogue PID feedback controller or a digital IMC feedback controller. In the analogue PID control experiment, the three control gains in equation (6) were determined by manual tuning to be $K_P = 0{\cdot}4$, $K_I = 1{\cdot}6$ and $K_D = 0{\cdot}0004$. Since the sign of K_D is positive it will provide extra damping for the first bending mode of the flexible beam, and thus will decrease the settling time. However, it was found that if a value of K_D is made too large, the transient response of the beam is dominated by the second bending mode. Because of the 180° phase shift between these two modes, as seen in Figure 1(b), a value of K_D increasing the damping of the first bending mode will decrease the damping of the second mode. Thus, if K_D is to large the second mode will effectively have a negative damping and the system will become unstable. Although there has been a number of *ad hoc* tuning rates for the PID controller such as Ziegler–Nicholas [15], most of which assume a well-damped plant response, there is no analytic method of adjusting the three parameters to obtain the

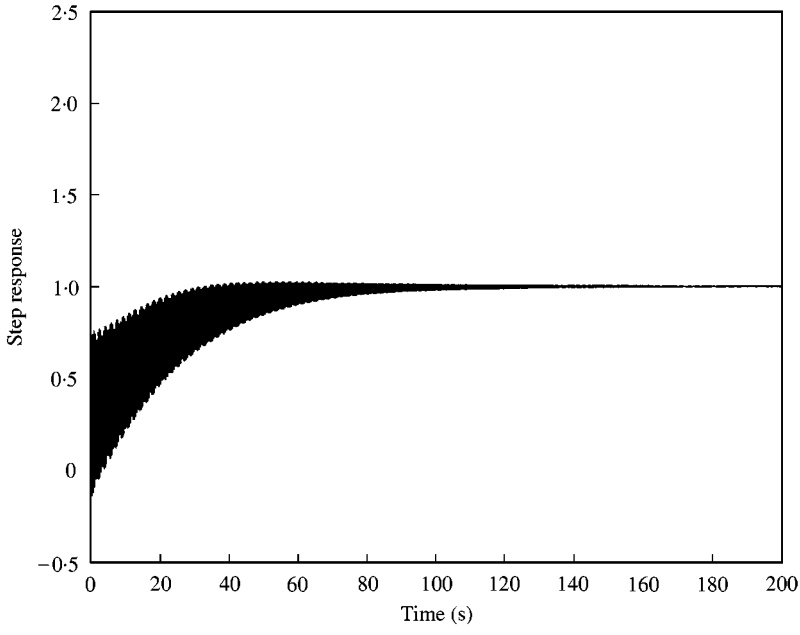

Figure 14. Measured step response with analogue PID feedback control.

shortest transient response. In this work, a trial and error approach was thus adopted to obtain the exact values of the gains about their final settings. The measured frequency response of the analogue PID feedback controller had an integration action as shown in Figure 4(d), determined by the K_I term, at very low-frequency range. The K_I term was chosen carefully because a higher K_I can provide an improved steady state tracking response but it can also cause a worse transient response. Figure 14 shows the measured closed-loop step response with the analogue PID feedback control, which settles to within 95 and 99% of the command position at about 75 and 120 s respectively. The measured step response is similar with the simulation result shown in Figure 4(b), but can be contrasted with the measured step response without control (95 and 99% settling times are 125 and 196 s) in Figure 1(c). In contrast, the measured step response with the analogue PID feedback controller shows that it follows the command gradually with limited overshoot using an electronic stiffness (by K_P and K_D of the controller) created by the piezoactuators. It settles precisely to the command position by the action of the gain K_I as can be seen from Figure 14. The piezoactuator with the controller has worked to generate bending moments used not only for the maintaining of the tip position but also for creating an electronic stiffness.

5.2. DIGITAL IMC FEEDBACK CONTROL

In the real-time IMC feedback control system, a digital signal processor (DSP) board (Loughborough Sound Images TMS320C30 PC system board [21]) based on TI's TMS320C30 (32-bit floating point operation) [22] with 16-bit ADC (analogue to digital converter)/DAC (digital to analogue converter) was used. The implementation flow for the digital IMC feedback control is illustrated in Figure 15. The digital plant model $\hat{G}(z)$ for the

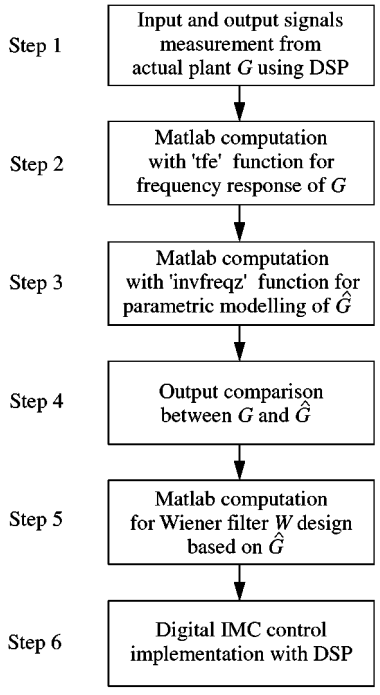

Figure 15. The implementation flow of digital IMC feedback control for the flexible beam.

sampled-time plant $G(z)$ has been defined to include the responses of a DAC, an antialiasing low-pass filter, a power amplifier, the physical flexible beam with a pair of piezoactuators, a tip position sensor, a reconstruction low-pass filter and an ADC. The sampling frequency was 300 Hz and the cut-off frequency in the low-pass filters was 100 Hz. Thus, the plant model $\hat{G}(z)$ on which the digital design is based must contain the inherent time delay caused by the DSP computation time and the low-pass filters' delay, as well as the pure delay in the non-minimum-phase flexible beam. The practical identification of the digital plant model is contained in step 1–3 of Figure 15. In "step 1" the input and output signals of the sampled-time plant $G(z)$ have been measured with the DSP board and at "step 2 and 3" MATLAB functions "tfe" and "invfreqz" were used for the parametric modelling of the plant model $\hat{G}(z)$. The calculated impulse response of $\hat{G}(z)$ was more than 65 000 samples long. Since such a long FIR filter was beyond the capabilities of the DSP device, $\hat{G}(z)$ was instead implemented as an IIR filter in the DSP board with 45 poles and 45 zeros. Since an IIR filter can be unstable, the stability of the designed $\hat{G}(z)$ was verified from its pole-zero map. This stability monitoring has been important, since the plant to be controlled was very flexible with low damping ratios, and the poles of the IIR plant model $\hat{G}(z)$ were located very near to the unit circle. In "step 4" the output of the actual plant $G(z)$, y, and the IIR plant model $\hat{G}(z)$ output, $\hat{y}$, were compared to verify the precision of the designed $\hat{G}(z)$. The error between the two outputs could be caused by the change of the actual plant due to temperature variation or unexpected ambient vibration transmitted to the beam set-up for instance. This error could arise because it requires some time to calculate the IIR plant model in a PC and to implement the IIR plant model to the DSP board after the measurement at "step 1". If this error was too large, the identification process was repeated. The digital IMC control filter $W(z)$ was designed in "step 5" using off-line computer

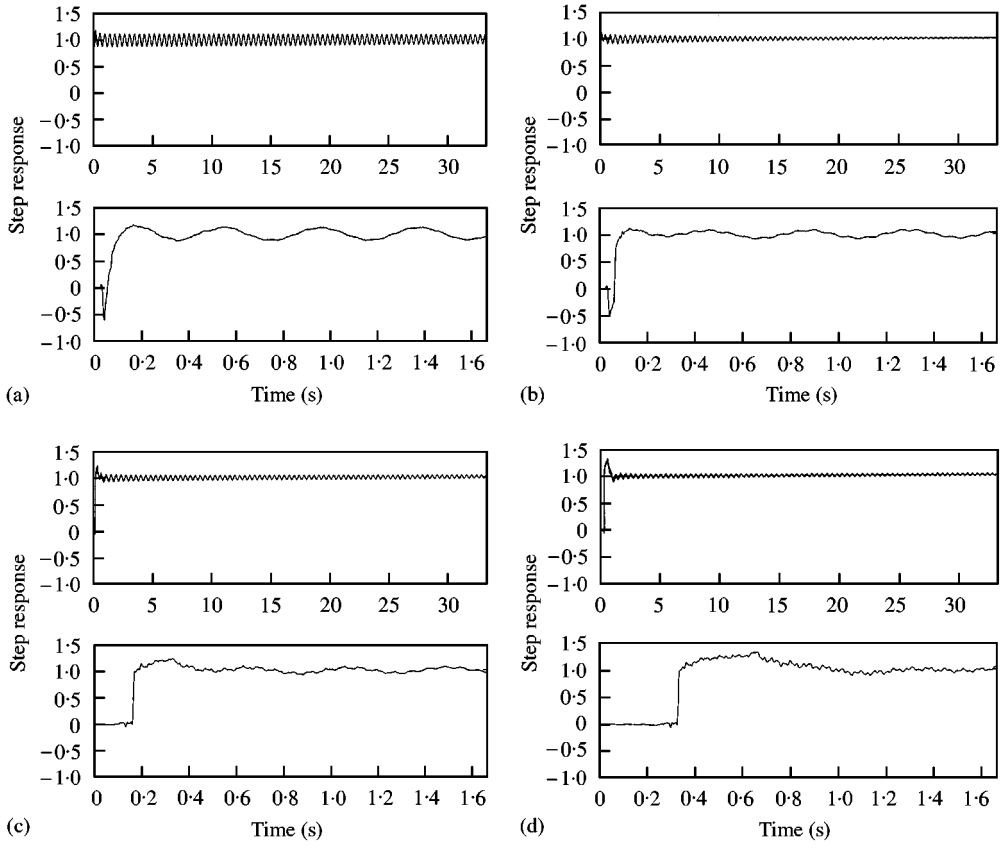

Figure 16. Measured step responses with a digital IMC position control. The control filter was designed with a Brownian noise input considering a modelling delay Δ. (a) $\Delta = 0$, (b) $\Delta = 20$, (c) $\Delta = 50$, (d) $\Delta = 100$.

calculations as given in equation (13) using the plant model $\hat{G}(z)$ and a Brownian noise input, with various modelling delays of $\Delta = 0$, 20, 50, and 100, and was implemented as an FIR device with 200 coefficients in the DSP board. The control effort weighting β has not been considered in the design of the control filter $W(z)$ since the simulation results have already indicated that effort weighting is not a useful concept in the position control of very lightly damped beams. After this design process, the complete real-time digital IMC feedback control system, as shown in Figure 2(b), could be implemented with the DSP board.

In the real-time control experiment, the IMC feedback control designed with these modelling delays has been implemented. The upper and the lower graphs in Figure 16(a), (b), (c), and (d) (when $\Delta = 0$, 20, 50 and 100, respectively), represent the measured real-time closed-loop step responses from 0 to 10 000 samples (about 0–33 s) and 0–500 samples (about 0–1·7 s) respectively. The closed-loop step response of the IMC feedback control with no modelling delay ($\Delta = 0$) did not settle within 95% of command position even after 33 s, as shown in Figure 16(a). However, the step responses with modelling delays Δ showed improved 95% settling times of 10·75, 10·93, and 2·60 s for $\Delta = 20$, 50 and 100, respectively, but the beam did not settle to within 99% of the desired result within 33 s, as can be seen from Figure 16(b)–(d). It should be noted, however, that 33 s is still short compared with the 196 s settling time of the beam itself, as shown in Figure 1(c).

The long settling times shown in Figure 16 for real-time control were probably caused by the misalignment in frequencies and magnitude differences between the anti-resonances of the control filter $W(z)$ and the resonances of the actual plant response $G(z)$; because the plant model was not perfect, $G(z) \neq \hat{G}(z)$. The misalignment at the first resonance frequency was dominant in the measured closed-loop step response with a ringing at about 2·4 Hz, as shown in Figure 16(a) when $\Delta = 0$. When $\Delta = 100$, the misalignment magnitude at the first resonance frequency became less significant but misalignments at the other resonances became increased, as shown in Figure 16(d). Each of the measured closed-loop step response in Figure 16 are quite similar to the calculated response in Figure 9(a) up to 500 samples.

The misalignment of the resonance frequencies of $G(z)$ and the anti-resonance frequencies of $W(z)$ may have been caused by slight changes in the plant dynamics. The actual plant dynamics $G(z)$ could be perturbed not only by temperature variation but also by small changes in the static geometry of the aluminium beam caused by plastic deformation by the piezoelectric actuators. The variation of the plant model $\hat{G}(z)$ over the course of these experiments showed that the mean value of the first natural frequencies was 2·3763 Hz and the standard deviation was 0·0018 Hz. This amount of variation in the first natural frequency does not destabilize the control system, but can cause the observed ringing in the closed-loop step response. This frequency misalignment problem can make the system unstable if it is too large, as shown by the tip mass perturbation results in Table 2. The system will only be stable if the error in the estimate of the natural frequency is less than about half the bandwidth of the resonance. The condition of stability with an IMC position control architecture for a flexible structure can thus be approximated by

$$|f_n - \hat{f}_n| < f_n \zeta_n, \tag{24}$$

where f_n and $\hat{f}_n$ are the nth natural frequencies of the actual plant $G(z)$ and plant model $\hat{G}(z)$, and ζ_n is the nth damping ration of the actual plant. If f_1 and ζ_1 are 2·3700 and 0·0026 Hz, then the frequency difference $|f_1 - \hat{f}_1|$ should be less than about 0·006 Hz for stability. For a stable IMC controller it also is necessary to use a minimum FFT resolution in "step 2 and 3" in the identification process which is smaller than $|f_n - \hat{f}_n|$ so that

$$N_{FFT} \geqslant f_s / f_n \zeta_n, \tag{25}$$

where f_s is the sample rate and N_{FFT} is the number of points in the FFT process. In practice $N_{FFT} = 100\,000$ was used.

From the above analysis it could be concluded that the precision of the plant model $\hat{G}(z)$ determines not only the stability but also the closed-loop performance for the position control of a very flexible beam with an IMC feedback control architecture. Even with a very small difference between the natural frequencies of the actual plant and of the plant model, the closed-loop response of the IMC feedback control system could suffer from ringing and a reduced tracking performance. The difficulty of implementing a practical IMC controller for a very lightly damped beam can thus be seen to be associated with the extreme precision of the coefficients of the IIR filter for the plant model. In addition, a very large FFT point as well as long-time measurements of input and output signals for the identification of the plant are necessary to reduce the misalignment problem in the calculation of $\hat{G}(z)$ and $W(z)$. It may be possible to reduce this misalignment by using on-line identification of the plant response and iterative re-design of the control filter, although it should be noted that the beam used in these experiments did have unusually light damping for practical engineering structures and many of the practical problems encountered would be avoided if a beam with a somewhat higher damping had been used.

6. CONCLUSION

This paper describes the design, simulation and implementation of an active position controller using internal model control (IMC) for setpoint tracking control of a smart flexible beam. The smart flexible cantilever beam was activated by a pair of piezoceramic actuators bonded at the clamped end on both sides of the beam. The objectives of the position controller for the smart flexible beam were to eliminate its long natural response, due to the very low damping ratio of the beam material, and to maintain a low steady state error by inverse control of the non-minimum phase plant. The optimum performance of a feedback control system was obtained by using quadratic optimization techniques based on the minimization of the mean-square tracking error. However, the smart beam could be perturbed by a temperature variation or the variation in the mass attached to the beam's tip. The robust stability was considered for perturbed plants. The performance and stability of the digital IMC feedback controller were compared with those of the analogue proportional integral derivative (PID) feedback controller. The digital IMC feedback control showed much better performance in settling time than that of the analogue PID feedback control. The analogue PID feedback controller was very robust but gave poor performance. The introduction of a modelling delay Δ into the design of the IMC control filter $W(z)$, gave a better performance and greater robust stability to the IMC feedback control system. An adaptive filter using the filtered-x LMS algorithm could also be used as a position controller, however, a very long adaptation time was required to learn the behaviour of the lightly damped flexible beam. In a practical implementation of the IMC position control, even a very small misalignment between the natural frequency of the actual plant and the anti-resonance frequency of the control filter could cause a ringing motion and a reduced tracking performance. However, a much faster settling was achieved with real-time digital IMC control than with analogue PID control.

REFERENCES

1. C. R. Fuller, S. J. Elliott and P. A. Nelson 1996 *Active Control of Vibration*. New York: Academic Press.
2. R. L. Clark, W. R. Saunders and G. P. Gibbs 1998 *Adaptive Structures Dynamics and Control*. New York: John Wiley & Sons.
3. E. Gross and M. Tomizuka 1994 *IEEE Transactions on Control Systems Technology* **2**, 382–391. Experimental flexible beam tip tracking control with a truncated series approximation to uncancelable inverse dynamics.
4. R. L. Wells, J. K. Schueller and J. Tlusty 1990 *IEEE Control Systems Magazine* **10**, 9–15. Feedforward and feedback control of a flexible robotic arm.
5. N. C. Singer and W. P. Seering 1990 *American Society of Mechanical Engineers Journal of Dynamic Systems, Measurement, and Control* **112**, 76–82. Preshaping command inputs to reduce system vibration.
6. M. Morari and E. Zafiriou 1989 *Robust Process Control*. Englewood Cliffs, NJ: Prentice-Hall.
7. S. J. Elliott and T. J. Sutton 1996 *IEEE Transaction on Speech and Audio Processing* **4**, 214–223. Performance of feedforward and feedback systems for active control.
8. E. F. Crawley and J. DE Luis 1987 *American Institute of Aeronautics and Astronautics Journal of Guidance and Control* **25**, 1373–1385. Use of piezoelectric actuators as elements of intelligent structures.
9. M. J. Brennan, S. J. Elliott and R. J. Pinnington 1997 *Journal of Acoustical Society of America* **102**, 1931–1942. The dynamic coupling between piezoelectric actuators and a beam.
10. Morgan Matroc Inc. 1993 *Guide to Modern Piezoelectric Ceramics*.
11. A. Papoulis 1984 *Signal Analysis*. New York: McGraw-Hill.
12. R. E. D. Bishop and D. C. Johnson 1960 *The Mechanics of Vibration*. Cambridge: Cambridge University Press.

13. D. K. MIU 1991 *American Society of Mechanical Engineers Journal of Dynamic Systems, Measurement, and Control* **113**, 419–424. Physical interpretation of transfer function zeros for simple control systems with mechanical flexibilities.
14. P. A. A. LAURA, J. L. POMBO and E. A. SUSEMIHL 1974 *Journal of Sound and Vibration* **37**, 161–168. A note on the vibrations of a clamped–free beam with a mass at the free end.
15. G. F. FRANKLIN, J. D. POWELL and A. EMAMI-NAEINI 1994 *Feedback Control of Dynamic Systems*, 3rd edition. Reading, Massachussets: Addison-Wesley.
16. B. WIDROW and S. D. STEARNS 1985 *Adaptive Signal Processing*. Englewood Cliffs, NJ: Prentice-Hall.
17. P. A. NELSON and S. J. ELLIOTT 1992 *Active Control of Sound*. New York: Academic Press.
18. J. C. DOYLE, B. A. FRANCIS and A. R. TANNENBAUM 1992 *Feedback Control Theory*. New York: Maxwell MacMillan International.
19. R. JOHANSSON 1993 *System Modeling Identification*. Englewood Cliffs, NJ: Prentice-Hall.
20. S. J. ELLIOTT, C. C. BOUCHER and P. A. NELSON 1992 *IEEE Transactions on Signal Processing* **40**, 1041–1052. The behavior of a multiple channel active control system.
21. Loughborough Sound Images Limited 1992 *TMS*320*C*30 *PC System Board Technical Reference Manual Version* 1.03.
22. Texas Instrument 1997 *TMS*320*C*3*X User's Guide*.